

A&A manuscript no.
(will be inserted by hand later)

Your thesaurus codes are:
03(11.04.4;11.06.2;11.16.1;04.03.1)

ASTRONOMY
AND
ASTROPHYSICS

The central region of the Fornax cluster – I. A catalog and photometric properties of galaxies in selected CCD fields

Michael Hilker^{1,4}, Markus Kissler-Patig^{2,1,3}, Tom Richtler¹, Leopoldo Infante⁴, and Hernan Quintana⁴

¹ Sternwarte der Universität Bonn, Auf dem Hügel 71, 53121 Bonn, Germany

² UCO/Lick Observatory, University of California, Santa Cruz, CA 95064, USA

³ Feodor Lynen Fellow of the Alexander von Humboldt Foundation

⁴ Departamento de Astronomía y Astrofísica, P. Universidad Católica, Casilla 104, Santiago 22, Chile

Received — / Accepted —

Abstract. We present a photometric catalog (based on V and I photometry) of galaxies in the central regions of the Fornax galaxy cluster. Our 11 CCD fields cover 0.17 square degrees in total. The limiting surface brightness is around 24 mag arcsec⁻², similar to that of Ferguson's (1989) catalog, whereas our limiting total magnitude is around $V \simeq 22$ mag, about two magnitudes fainter. It is the surface brightness limit, however, that prevents us from detecting the counterparts of the faintest Local Group dwarf spheroidals. The photometric properties of all objects are presented as a catalog (Appendix A)¹. The properties and fit parameters of the surface brightness profiles for a sub-sample are presented as a second catalog (Appendix B)¹.

We can only add 4 new dwarf galaxies to Ferguson's catalog. However, we confirm that the dwarf galaxies in Fornax follow a similar surface brightness – magnitude relation as the Local Group dwarfs. They also follow the color (metallicity) – magnitude relation seen in other galaxy clusters. A formerly suspected excess of dwarf galaxies surrounding the central giant cD galaxy NGC 1399 can finally be ruled out.

An enhanced density of objects around NGC 1399 can indeed be seen, but it appears displaced with respect to the central galaxy and is identified as a background cluster at $z = 0.11$ in Paper II of these series, which will discuss spectroscopic results for our sample.

Key words: galaxies: clusters: individual: Fornax cluster – galaxies: fundamental parameters – galaxies: photometry – catalogs

1. Introduction

The galaxy population in the Fornax cluster is well studied down to a B magnitude of 19 mag by the photographic survey of Ferguson (1989) which resulted in the Fornax Cluster Catalog (FCC). In addition, Davies et al. (1988) and Irwin et al. (1990) provided a catalog of the (very) low surface brightness galaxies in this region, which then also have been studied by follow-up CCD photometry (Bothun et al. 1991, Cellone et al. 1996).

The photographic data of Ferguson (1989) were obtained on the same telescope as the present study. In Ferguson's survey a diameter limit of 17'' was chosen to reduce the number of background galaxies. In our CCD survey galaxies with smaller scale lengths were included in order to search for compact dwarf galaxy, e.g. similar to M32, and to extend the galaxy counts to fainter absolute magnitudes. Furthermore, CCD photometry provides the possibility to search for objects in the immediate environment of giant galaxies (where the galaxy light dominates) when adopting appropriate reduction techniques.

Our main goal is to find dwarf galaxies in the vicinity of giant ellipticals in the Fornax cluster, especially the central galaxy NGC 1399. One striking characteristic of NGC 1399 (and other central galaxies in clusters) is its extraordinarily rich globular cluster system (GCS), whose origin is a matter of lively debate. Several authors investigated photometric and spectroscopic properties of the GCS (e.g. Hanes & Harris 1986; Bridges et al. 1991; Wagner et al. 1991; Grillmair et al. 1994; Kissler-Patig et al. 1997, 1998a,b; Forbes et al. 1998). Further, NGC 1399 possesses an extended cD halo (Schombert 1986; Killeen & Bicknell 1988), which seems to be typical for the brightest cluster galaxies of dynamically evolved clusters (López-Cruz et al. 1997). The building-up of such a rich GCS as well as the formation of a cD halo are not well understood. Both properties might be related to the infall of dwarf galaxies in the cluster center. A more detailed discussion on this topic will be given in Paper III of this series (Hilker et al. 1998).

Send offprint requests to: M. Hilker

Correspondence to: mhilker@astro.uni-bonn.de

¹ The tables of Appendix A and Appendix B are only available in electronic form at the CDS via anonymous ftp to cdsar.u-strasbg.fr (130.79.128.5) or via <http://cdsweb.u-strasbg.fr/Abstract.html>

Fig. 1. Image taken from the Digital Sky Survey, showing the observed CCD fields in the Fornax cluster. Field B2 lies outside this image to the east

In the present paper the photometric properties of all galaxies found in the observed fields are cataloged. The identification, classification and the photometry of the objects as well as the completeness of our counts are described. Furthermore, we present the spatial and the color distribution of the galaxies as well as the surface brightness profile parameters of a subsample of galaxies with a sufficient resolution in their angular diameters. In this paper we adopt a distance to the Fornax cluster of 18.2 Mpc or $(m - M)_0 = 31.3$ mag (Kohle et al. 1996, recalibrated with new distances of Galactic GCs, Gratton et al. 1997, following Della Valle et al. 1998). The spectroscopy and the determination of radial velocities of the brightest galaxies in our sample represents the topic of a second paper (Hilker et al. 1998, hereafter Paper II).

2. Selection of the observed fields

2.1. Observed fields

We selected 11 fields in the Fornax cluster which comprise giant galaxies as well as control fields without any bright Fornax galaxy. A mosaic of 4 fields matches the central giant elliptical NGC 1399 (named F1, F2, F3, and F4 as shown in Fig. 1). Five other target galaxies are the giant ellipticals NGC 1374, NGC 1379, and NGC 1427, the S0

galaxy NGC 1387, and the irregular NGC 1427A. The 2 additional fields (named B1 and B2 in the following) are located 13' and 95' east of NGC 1399, respectively. Note that field B2 is not suitable for an estimation of the absolute galaxy background, since it still lies in a region where Fornax member galaxies contribute to the galaxy counts, as seen in the radial density profiles of Ferguson (1989). All fields, except B1 and the four NGC 1399 fields, can serve as relative backgrounds to identify a possible excess population near NGC 1399 with respect to the “normal” Fornax field galaxies. In total, our fields cover an area of about 600 square arcmin (or 0.17 square degree). Figure 1 is an extraction of the Digital Sky Survey and shows the location of all our fields except B2.

In a second observing run, 2 additional outlying background fields 10° north (B3) and 15° south of NGC 1399 have been observed (see Sect. 3.1).

2.2. Nomenclature of catalog fields

In the following the acronym CGF (Catalog of Galaxies in Fornax) will be used for the nomenclature of galaxies in the observed fields followed by a sequence number of the field and the sequence number of the galaxy in this field ordered by decreasing magnitude. For example, CGF 5-12 is

the 12th brightest galaxy in field 5. The sequence numbers of the fields are ordered with increasing distance to the center of the Fornax cluster. The cross references to the CCD fields as described above are (see also Fig. 1): CGF 1 = F1 (NGC 1399, SE field), CGF 2 = F2 (NGC 1399, NE field), CGF 3 = F3 (NGC 1399, SW field), CGF 4 = F4 (NGC 1399, NW field), CGF 5 = B1, CGF 6 = NGC 1387, CGF 7 = NGC 1427A, CGF 8 = NGC 1379, CGF 9 = NGC 1374, CGF 10 = NGC 1427, and CGF 11 = B2.

3. Observations and Reduction

The observations were performed with the 2.5m DuPont telescope at Las Campanas Observatory, Chile, in the nights of 26-29 September, 1994. A Tektronix 2048 × 2048 pixel chip has been used, with a pixel size of 21 μm or 0''.227 at the sky, corresponding to a total field of view of 7'.7 × 7'.7.

Deep exposures in Johnson V and Cousins I were acquired. Typical total exposure times are between 30 min and 60 min per field in both filters. The seeing, given as the full width at half maximum (FWHM) of a Gaussian profile, ranged between 0''.9 and 1''.5. The exposures of the south-west field of the NGC 1399 mosaic were affected by a tracking jump in one long V exposure and the corruption of one long I exposure. Omitting these two exposures the total exposure time was reduced to 15 min in both filters. Nevertheless, this field has been considered in several aspects of our investigations since it contains some interesting bright galaxies. For the photometric calibration typically 15–30 standard stars from the Landolt (1992) list have been observed throughout the nights.

Table 1 summarizes the observations. In addition, the detection threshold μ_{limit} in mag arcsec⁻² in V and I is given for each field (see also Sect. 4). For more information about the calibration see Kissler-Patig et al. (1997).

Bias subtraction, flat-fielding, long exposures combination, modelling, and subtraction of the galaxy light of the giants were done with IRAF (for details see Kohle et al. 1996 and Kissler-Patig et al. 1997). After these procedures frames with flat backgrounds ready for object search and photometry were obtained.

3.1. Background fields

To get an estimation of the absolute background galaxy counts two additional fields 10° north (B3) and 15° south (B4) of NGC 1399 have been observed. The total magnitudes and colors of the galaxies have been determined for a statistical comparison with the photometric properties of galaxies in the Fornax fields. The surface brightness (SB) profiles have not been measured, because the resolution of the images is 3 times lower than in the run at the 2.5m telescope.

The observations have been performed in a second run with the 1.0m Swope telescope at Las Campanas Observa-

Table 1. The observations of the Fornax fields obtained with the 2.5m telescope and the background fields obtained with the 1.0m telescope on Las Campanas. In addition, the surface brightness threshold μ_{limit} in mag arcsec⁻², above which objects of at least five connected pixels are detected, is given for each field

Field & Filter	Date	Exp. time [s]	Seeing [']	μ_{limit} [mag/□']	
NGC 1374	V	28.9.94	2 × 1200	1.2	25.0
	I	29.9.94	1200	1.5	24.2
			+2 × 600		
NGC 1379	V	29.9.94	2 × 1200	1.2	25.4
	I	26.9.94	3 × 1200	1.4	24.7
NGC 1387	V	28.9.94	2 × 900	1.3	24.8
	I	28.9.94	2 × 900	1.2	23.5
NGC 1427	V	26.9.94	3 × 1200	1.5	25.3
	I	26.9.94	3 × 1200	1.3	24.6
NGC 1427A	V	28.9.94	2 × 900	0.9	25.1
	I	28.9.94	2 × 900	0.9	24.0
NGC 1399 F1	V	27.9.94	2 × 900	0.9	24.7
	I	27.9.94	2 × 900	1.1	24.1
NGC 1399 F2	V	27.9.94	2 × 900	0.9	24.8
	I	27.9.94	2 × 900	1.3	24.1
NGC 1399 F3	V	28.9.94	1 × 900	1.2	24.3
	I	28.9.94	1 × 900	1.2	22.1
NGC 1399 F4	V	28.9.94	2 × 900	1.0	24.9
	I	28.9.94	2 × 900	1.1	24.3
B1	V	29.9.94	2 × 900	1.1	25.2
	I	29.9.94	2 × 900	1.1	24.0
B2	V	29.9.94	2 × 900	1.0	25.3
	I	29.9.94	2 × 900	1.2	24.0
B3	V	2.12.96	3 × 1200	1.5	26.0
	I	2.12.96	3 × 1200	1.5	24.5
B4	V	2.12.96	3 × 1200	1.6	25.5
	I	2.12.96	3 × 1200	1.7	24.2

tory, Chile, in the night of 2/3 December, 1996. A SItE#1 2048 × 2048 pixel chip has been used, with a pixel size 0''.694 at the sky, corresponding to a total field of view of 23'.69 × 23'.69. Table 1 (at the bottom) gives an observation log of the V and I exposures. As in the first run the photometric calibration was done via standard stars from the Landolt (1992) list.

4. Object detection and photometry

The identification, photometry and classification of the objects have been performed with the program SExtractor (Source-Extractor, Bertin 1995).

First, a background map was constructed and subtracted from the image. The sky map is a bilinear interpolation between the meshes of a grid with a mesh size of 56 × 56 pixel (or 128 × 128 pixel in the case of the more

extended Fornax dwarf ellipticals). In addition, a median filter of 5×5 pixel has been applied in order to suppress possible overestimations due to bright stars. Then the image was convolved with a Gaussian with a FWHM slightly larger than that for stellar images in order to favour the detection of marginally resolved objects. A FWHM of $2''$ was chosen for all fields except the background fields B3 and B4, which were convolved with a Gaussian of $1''.5$ FWHM. Objects were found with a threshold of about 2 sigmas above the sky level. The level of the lowest isophote in V and I above which objects were detected is given in Table 1 for the different fields. The minimum number of connected pixels for a detection was chosen to be 5 in all fields. Composite objects were deblended by a multithresholding algorithm. In all fields the identifications have been controlled by eye, obvious multi-identifications of the same object were removed and objects that had been missed by the finding algorithm were added. The number of added objects was always below 2% of the total number.

The finding completeness starts to drop in V at magnitudes between 22.0 and 22.5 mag (except the NGC 1399 SW field: 21.0) and in I at magnitudes between 21.0 and 21.5 mag (NGC 1399 SW field: 20.0) depending on the seeing and exposure times of the different fields. The finding limit for low surface brightnesses varies between 23.0 and 24.0 mag arcsec $^{-2}$ peak surface brightness in V (μ_{peak} is the surface brightness of the central pixel as given by SExtractor). This latter limit is about the same as in the FCC, whereas the limiting total magnitude is about 2 magnitudes fainter than in the FCC.

The photometry was done via elliptical apertures whose ellipticity and position angle are defined by the second order moments of the light distribution. Total magnitudes are computed in two different ways. For isolated objects the flux is measured within an aperture calculated by a further development of Kron’s “first moment” algorithm (Kron, 1980; see also Infante 1987). For overlapping objects, i.e. which have neighbours within the elliptical aperture, the fraction of flux lost by the isophotal magnitude (using the detection threshold as the lowest isophote) is estimated and corrected assuming that the intensity profiles have gaussian wings because of atmospheric blurring.

The color determination was done by measuring aperture magnitudes from circular apertures with $3''$ diameter in both filters. Peak surface brightnesses (μ_{peak} in mag arcsec $^{-2}$) are calculated from the peak intensity at the central pixel. Note that for objects with apparent core radii intrinsically smaller than the seeing the derived central surface brightness is a lower limit compared to the true central surface brightness due to the convolution with the seeing. A more detailed analysis of the surface brightness profiles of the brighter galaxies in our sample is given in Sect. 6.

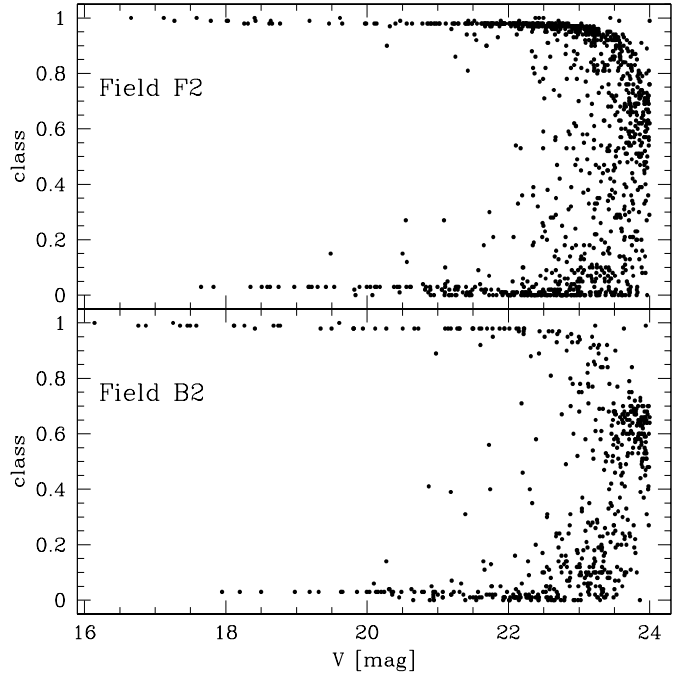


Fig. 2. The classifier value (0 = galaxy, 1 = point source) is plotted versus the V magnitude for two different CCD fields (see Fig. 1). For $V < 21$ the separation of point sources and galaxies is obvious. For fainter magnitudes all objects with classifier values below 0.35 have been identified as well resolved. Note that most point sources in field F1 are globular clusters that belong to the central galaxy NGC 1399

The photometric calibration was done by applying the calibration equations for aperture photometry given in Kissler-Patig et al. (1997).

5. Classification and selection

The separation of resolved (= galaxies) and unresolved (= stars, globular clusters, and unresolved background galaxies) was done with the “star/galaxy classifier” developed by Bertin & Arnouts (1996). It is a neural network trained program that classifies each object with a “stellarity index” between 0 (galaxy) and 1 (point source). In all fields the separation works fine down to a V magnitude of 21 mag. Beyond this magnitude the classifier values start to scatter. Figure 2 shows as an example the classifier versus V magnitude plots for the NE field (F2) of NGC 1399 and the background field B2. Eye control in all fields showed that all objects with classifier values below 0.35 are well resolved objects, whereas objects above this value can not be clearly classified.

Therefore all objects were selected that have classifier values below 0.35. Down to a $V_{\text{tot}} = 22.0$ and 23.0 mag we found 873 and 1775 galaxies respectively. The properties of all galaxies brighter than 22.0 mag are compiled in a catalog, see Appendix A. This cutoff in the final sample

was chosen for several reasons: the finding completeness starts to drop, the scatter in the classifier values increases significantly. Also, at this magnitude we would not find any dEs that follow the surface brightness – magnitude relation of Local Group or Virgo dwarf spheroidals (e.g. Kormendy 1985, Binggeli 1994) due to the limit in surface brightness. See Sect. 7 for a discussion of the completeness of dwarf galaxies in the Fornax distance.

In the background fields B3 and B4 we found with the same selection criteria 668 and 1022 down to $V = 22.0$ mag respectively. However, one has to be careful when comparing these results with those of the other CCD fields. The pixel size is about 3 times larger than in the first run leading to a 9 times higher area covered by each pixel. We simulated this resolution for two fields of our first run by binning 3×3 pixel and run SExtractor again. On the one hand, some galaxies have been classified as point sources due to their small angular sizes below the “new” resolution. On the other hand, some new “galaxies” have been gained due to the overlap of objects very close in the high resolution image. Down to our magnitude limit of $V = 22.0$ mag loss and gain of galaxies are nearly balanced and in the order of 8% of the total galaxy counts.

6. Surface brightness profiles

In combination with the morphological appearance of the observed galaxies, the analysis of their SB profiles provides a reliable tool to classify them as cluster dwarf galaxies or background galaxies (e.g. Sandage & Binggeli 1984). In the surface brightness versus magnitude diagram (μ - V diagram) the dEs follow a well defined sequence.

A growth curve analysis for each galaxy has been made with increasing elliptical apertures using the position, ellipticity, and position angle of the SExtractor photometry results. As local background the SExtractor value of the interpolated sky map for each individual galaxy was taken (see Sect. 4). In some cases overlapping stars have been removed before the analysis by interpolating the galaxy surface brightness profile from a unaffected ring outside the stellar profile. In other cases, the region of an overlapping star was masked out during the fitting process of the surface brightness profile. Two model-independent parameters have been determined for the galaxies: the effective semi-major axis a_{eff} (major axis of the ellipse that contains half of the total light) and the mean effective surface brightness within the effective semi-major axis, $\langle \mu_{\text{eff}} \rangle = V_{\text{tot}} + 5 \cdot \log(a_{\text{eff}}) + 2.5 \cdot \log(2\pi(1 - \epsilon))$, with $\epsilon = 1 - b/a$ ($b =$ semi-minor axis, $a =$ semi-major axis). These parameters, as well as the size of the full major axis D_{26} at the isophote of $V = 26$ mag arcsec $^{-2}$, are given in the photometric catalog (Appendix A).

The $\mu_{\text{eff}}-V_{\text{tot}}$ is shown in Fig. 3 (middle panel). Qualitatively, this plot is comparable to the $\mu_{\text{peak}}-V_{\text{tot}}$ diagram in the upper panel. The sequence of dwarf galax-

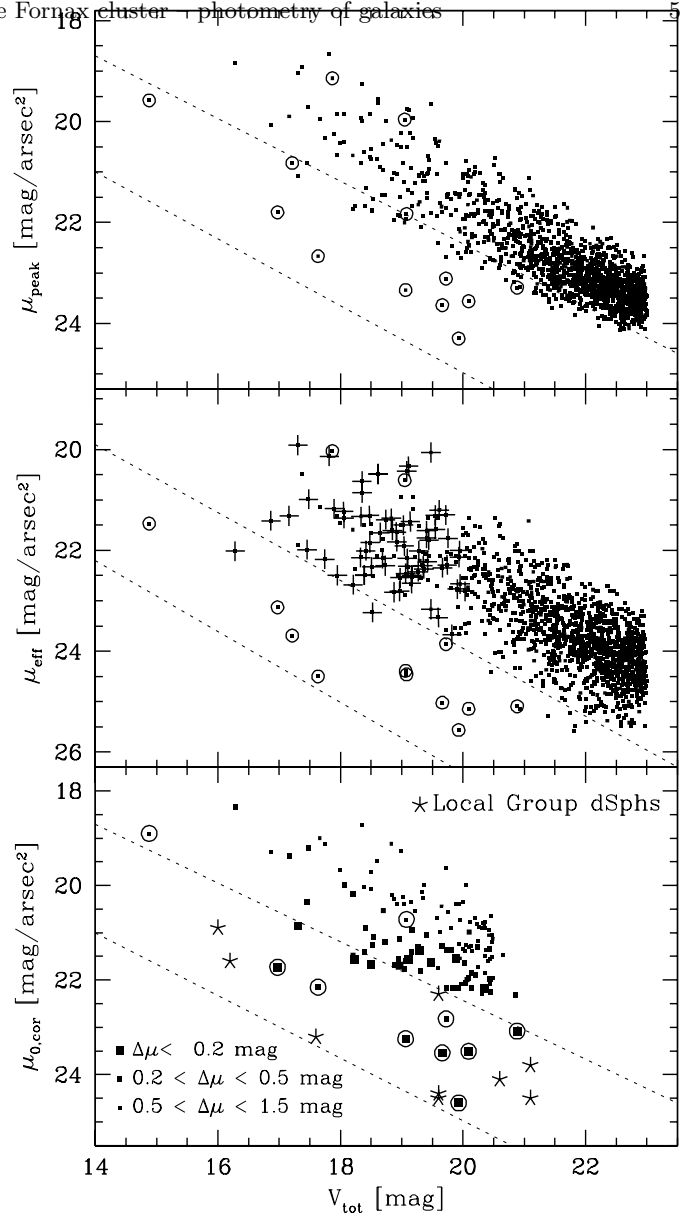


Fig. 3. The three panels show surface brightness versus total magnitude plots for all objects in the photometric catalog (small dots). In the upper two panels μ_{peak} (not seeing corrected) and μ_{eff} from growth curve analyses are plotted. In the lower panel the corrected central surface brightness (as described in the text) is shown for a subsample of galaxies. $\Delta\mu$ is the difference between the apparent and corrected central surface brightness. In all diagrams the encircled dots indicate Fornax cluster members, as follows from their radial velocity (see Paper II) and/or SB profile (Sect. 6). All other objects that are not encircled are suspected to be background galaxies. In the middle panel definite background galaxies, according to their radial velocities, are symbolised with crosses. In all panels the dotted lines mark the region that is defined by the μ - V relation of the Local Group and Virgo dEs (the asterisks in the lower panel are Local Group dSphs shifted to the Fornax distance; Kormendy 1985, Mateo et al. 1993).

Table 2. Photometric properties and profile fit parameters of dwarf galaxies in Fornax. The classification as dwarf galaxy is based on the morphological appearance, surface brightnesses, and in four cases on radial velocities.

Id	FCC	Type	RA(2000) [^h : ^m : ^s]	Dec(2000) [[°] : ['] : ^{''}]	V [mag]	$(V - I)$ [mag]	μ_{peak} [mag/□ ^{''}]	D_{26} [^{''}]	μ_{eff} [mag/□ ^{''}]	a_{eff} [^{''}]	$\mu_{0,\text{exp}}$ [mag/□ ^{''}]	α [^{''}]
CGF 9-6	145	dE	3:35:05.48	-35:13:06.5	19.06	1.03	23.34	16.6	24.39	5.2	23.44	3.6
CGF 9-12	154	dE	3:35:30.48	-35:15:05.9	20.09	0.99	23.56	17.0	25.14	6.7	24.30	5.6
CGF 8-1	160	dE,N	3:36:03.94	-35:23:20.5	17.63	1.05	22.67	34.0	24.50	12.2	23.36	7.2
CGF 8-3	162	dE	3:36:06.55	-35:25:54.5	19.66	0.89	23.64	12.0	25.02	5.0	24.16	3.5
CGF 6-5		dE,N	3:36:58.50	-35:29:45.5	19.08	0.98	21.83	20.0	24.46	7.6	23.93	6.3
CGF 4-1	202	dE,N	3:38:06.54	-35:26:24.4	14.88	1.34	19.58	64.0	21.47	10.7	20.48	6.7
CGF 3-1	B1241	dE/dS0	3:38:16.67	-35:30:27.9	16.97	0.93	21.80	38.0	23.13	8.7	22.11	5.3
CGF 3-2	208	dE,N	3:38:18.71	-35:31:52.1	17.21	1.12	20.82	35.6	23.69	8.5	22.98	6.6
CGF 1-44		dE	3:38:42.26	-35:33:08.2	20.88	0.82	23.29	12.0	25.09	6.7	23.97	3.2
CGF 1-4		cE/GC?	3:38:54.05	-35:33:33.9	17.87	1.12	19.14	11.2	20.03	1.1		
CGF 5-4		cE/GC?	3:39:35.92	-35:28:24.9	19.10	1.05	19.96	7.5	20.61	0.8		
CGF 10-13	272	dE	3:42:10.91	-35:26:32.5	19.93	0.58	24.30	12.0	25.56	6.5	24.94	6.3
CGF 10-11		dI?	3:42:16.11	-35:20:21.0	19.72	0.92	23.11	10.2	23.86	2.9	22.76	2.1

ies is clearly separated from the location of background galaxies. However, the nucleated dEs, that are hidden in the μ_{peak} plot among the background galaxies, fall in the range of the dE sequence when measuring μ_{eff} . In both diagrams, there are some galaxies located below the bulk of background galaxies, falling in the range of dwarf ellipticals. Each individual galaxy in this region has been individually inspected. Most of them are background spirals or galaxies that have close neighbours which disturb the correct μ_{eff} calculation. Furthermore, radial velocity measurements have shown that nearly all galaxies at the bright μ limit of the dE sequence are indeed background objects (see crosses in the middle panel of Fig. 3).

The determination of the true central surface brightness μ_0 is critical for objects with small angular diameters. The centrally peaked light distributions are blurred by seeing, which leads to a dimming of μ_0 . If the apparent core radius, where the surface intensity has decreased by a factor of 2 from its central apparent value, is smaller than $2\sigma_*$ ($\sigma_* = FWHM/2.354$), the SB profile cannot be deconvolved from the seeing profile (Schweizer 1981, Kormendy 1985). In our observations the average seeing dispersion is about $\sigma_* = 0''.45$.

In the following, the calculations are restricted to a subsample of galaxies, whose apparent core radii $r_{\text{c,app}}$ are larger than $0''.9$. The corrections given by Kormendy (1985) were applied to derive true core radii and true central surface brightnesses $\mu_{0,\text{cor}}$. Note that for objects with $r_{\text{c,app}} = 0''.9$ the correction for the true central surface brightness is of the order of 2 magnitudes, and the true core radius is about a third of the apparent one. At the distance of the Fornax cluster $0''.9$ corresponds to about 80 pc. The Local Group dSphs, for example, have core radii between 150 and 600 pc (Caldwell et al. 1992, Mateo et al. 1993). Thus, the apparent surface brightnesses of dEs

in the Fornax cluster should be nearly identical with their true central surface brightnesses, whereas compact dwarfs (like M32) and background galaxies are severely underestimated in their measured μ_{peak} . The core radius of M32, for example, is about 500 times smaller than that of Local Group and Virgo dEs ($\simeq 1\text{-}2$ pc, Kormendy 1985). Figure 3 (lower panel) shows the $\mu_{0,\text{cor}} - V_{\text{tot}}$ for all galaxies with corrections less than 1.5 mag. The different symbol sizes divide the sample in degrees of resolution of the core, as given by the ratio $r_{\text{c,app}}/\sigma_*$, which can directly be translated into the correction in magnitudes $\Delta\mu$: $\Delta\mu < 0.2$ mag corresponds to $r_{\text{c,app}}/\sigma_* > 5$, $\Delta\mu < 0.5$ mag to $r_{\text{c,app}}/\sigma_* > 3$, and $\Delta\mu < 1.5$ mag to $r_{\text{c,app}}/\sigma_* > 2$.

All non-nucleated Fornax cluster dwarfs are clearly separated from the bulk of background galaxies and fit the sequence of the Local Group dSphs. Their parameters are listed in Table 2. However, three well resolved background galaxies between $17 < V < 19$ mag also fall in this range. Visual inspection of these objects showed that they all are spirals seen edge-on. The surface brightness of edge-on spirals appears to be very low due to the light absorption by dust in the plane of their disks.

Most of the galaxies that are located in the dwarf region are already listed in the FCC (see Table 4, Appendix A, for cross references). Only 4 additional galaxies are probably dwarfs in the Fornax cluster due to their morphological appearance and their photometric properties. Their catalog names are: CGF 6-5, CGF 1-44, CGF 3-1, and CGF 10-11.

CGF 6-5 is located close to NGC 1387 and is visible only after subtraction of the galaxy light of NGC 1387. It looks like a nucleated dwarf elliptical judged from its surface brightness profile (see Fig. 4 lower left panel). CGF 1-44 is a dwarf elliptical south-east of NGC 1399. CGF 3-1 is listed in the catalog of probable background galaxies by

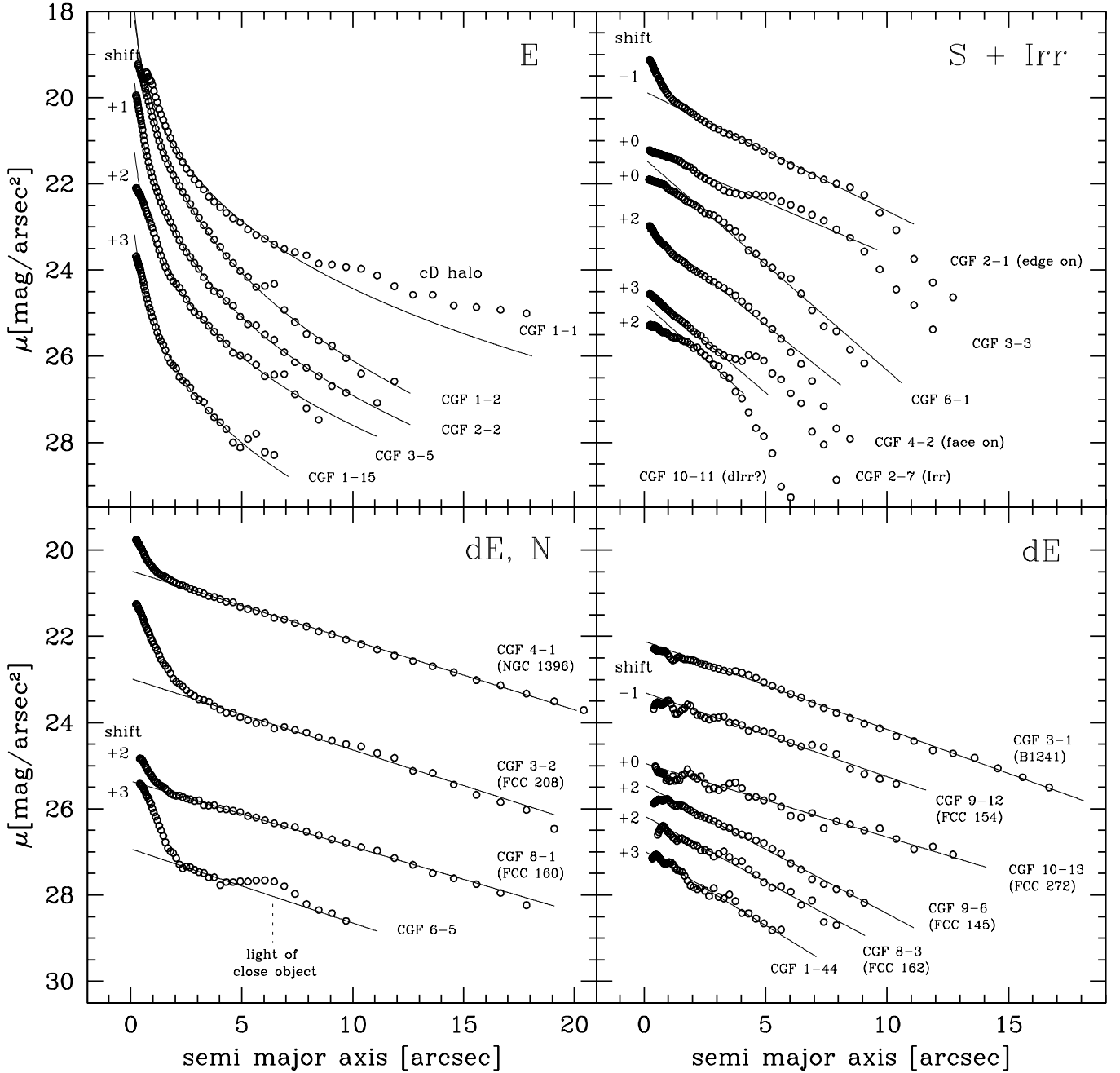


Fig. 4. Typical SB profiles of different galaxy types are shown in the four panels. For better illustration most profiles are shifted in μ as indicated by the numbers. The labels are the catalog names of this paper, cross references of the FCC catalog are given in parenthesis. In the upper left panel ellipticals are plotted together with de Vaucouleurs profile fits. The elliptical CGF 1-1 has a cD halo and is the brightest galaxy of a background galaxy cluster behind NGC 1399. The upper right panel shows the profiles of 4 spirals and 2 irregular galaxies with exponential fits to their disk components. In the lower panels, all galaxies that have been classified as nucleated and non-nucleated dEs (see Table 2) are shown

Ferguson (1989). According to our results this galaxy more likely resembles a dwarf elliptical or dwarf spheroidal in the Fornax cluster. CGF 10-11, located about $3\frac{1}{5}$ north of NGC 1427, has an irregular shape and a quite blue color $(V - I) = 0.9$ mag. According to its surface brightness it

is most likely a dwarf irregular. Nevertheless, this galaxy would be very small if it would belong to the Fornax cluster, and therefore might be a background object.

Two objects with very high surface brightness have been identified as Fornax members due to their radial ve-

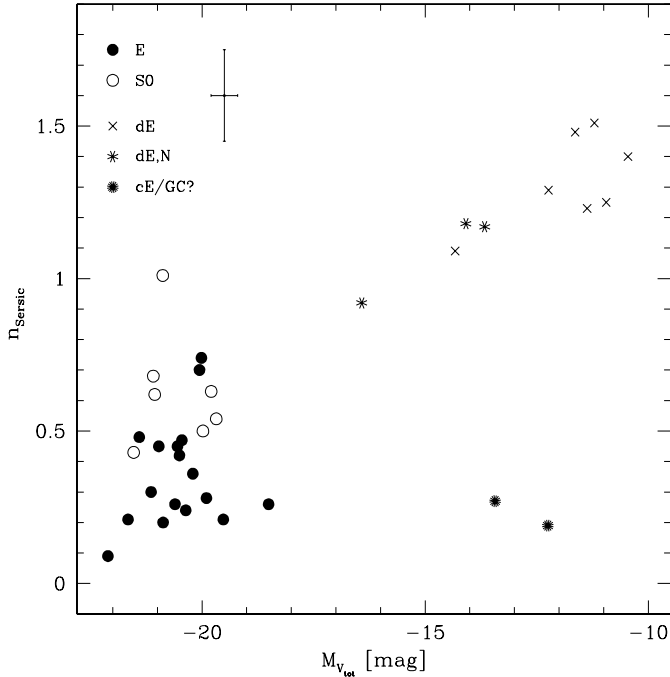


Fig. 5. The “n” parameter of the Sérsic profile fits is plotted versus the total absolute V magnitude for early-type galaxies. Filled and open circles indicate ellipticals and S0 galaxies from our spectroscopic sample (Paper II). Crosses are dwarf ellipticals, asterisks nucleated ones. The two dense asterisks in the lower right are the two compact objects found in the Fornax cluster. A typical error for the data points is given in the upper left. For the dwarf galaxies a n -luminosity relation is clearly visible

locity (see Paper II). As discussed in more detail in Paper II, these objects might be stripped nucleated dwarf ellipticals or very bright globular clusters. These examples show that compact objects at the Fornax distance can hardly be distinguished in their photometric properties from bulges of background spirals or ellipticals. More compact Fornax objects might be hidden in our galaxy sample. The photometric properties and profile fitting parameters of the galaxies that has been classified as Fornax members due to their morphological appearance, surface brightness – magnitude relation or radial velocity are given in Table 2.

Three different light profiles were fitted to a subsample of our galaxies that have major axis diameters larger than $D_{26} = 7''$. Depending on the shape of the SB profile type, an exponential law, a $r^{1/4}$ -law (de Vaucouleurs 1948) and/or a generalized exponential law were fitted to the outer part of the profiles, which are nearly unaffected by seeing effects. The innermost radius limit for all fits was $1''.5$. In Fig. 4 selected surface brightness profiles and their fits are shown. The upper panels give typical examples for background ellipticals, spirals and irregulars. The lower panels show all profiles of the Fornax cluster

nucleated and non-nucleated dEs from Table 2. The morphological types of the galaxies were not only determined on the basis of the profiles themselves, but also on properties like color, ellipticity, small scale structure (i.e. spiral arms, knots, etc.), and spectral informations (see Paper II). However, with decreasing angular diameter of the galaxy the morphological classification becomes more and more uncertain. Therefore, all type classifications with a “?” behind (Appendix B) should be taken with caution; they are more a guess than a certain determination.

The ellipticals have been fitted by a de Vaucouleurs profile of the form

$$I(r) = I_0 \exp(-7.67(r/r_{\text{eff}})^{1/4}) \text{ or} \\ \mu(r) = \mu_0 + 8.328(r/r_{\text{eff}})^{1/4},$$

μ_0 being the central surface brightness and r_{eff} the effective radius where the surface brightness is half the central value. In addition, we fitted the profiles of all early-type galaxies (Es, S0s, and dEs) by the generalized exponential law (Sérsic 1968)

$$I(r) = I_0 \exp(-r/\alpha)^n \text{ or} \\ \mu(r) = \mu_0 + 1.086(r/\alpha)^n, \quad n > 0,$$

which has been shown to describe the observed profiles much better (e.g. Graham et al. 1996). Furthermore, it is under discussion whether the exponent “n” of the Sérsic fit can be used as luminosity indicator. Young & Currie (1994) found that an n -luminosity relation exists for early-type dwarf galaxies. Jerjen & Binggeli (1997) suggested that this relation even is continued towards “normal” ellipticals. In Fig. 5 we show the “n” parameter plotted versus the absolute luminosity $M_{V, \text{tot}}$ for all Fornax dwarf elliptical in our sample and the early-type galaxies of our spectroscopic sample (see Paper II). The absolute luminosities were determined by adopting a distance modulus of $(m - M)_0 = 31.3$ mag to the Fornax dwarfs, and using the radial velocity and a Hubble constant of $H_0 = 70$ for the other galaxies. Whereas the scatter of “n” for the brighter galaxies is quite large due to the small angular diameter of the surface brightness profiles, the n -luminosity relation for the dwarf galaxies is clearly visible. The two compact Fornax objects do not follow the relation, but have “n” values comparable to ellipticals.

Spiral galaxies, S0s, dwarf ellipticals, and irregulars were fitted in the outer (disk) part by an exponential law,

$$I(r) = I_0 \exp(-r/r_D) \text{ or} \\ \mu(r) = \mu_0 + 1.086(r/r_D),$$

r_D being the characteristic radius where I_0 has decreased by a factor of e^{-1} . For some galaxies the inner part of the profile exceeds the fitted exponential law in brightness indicating the presence of a bulge or nucleus. Other galaxies show a light deficiency in the center, which might be due to seeing effects or due to dust. All fitting parameters are summarized in a catalog, Appendix B.

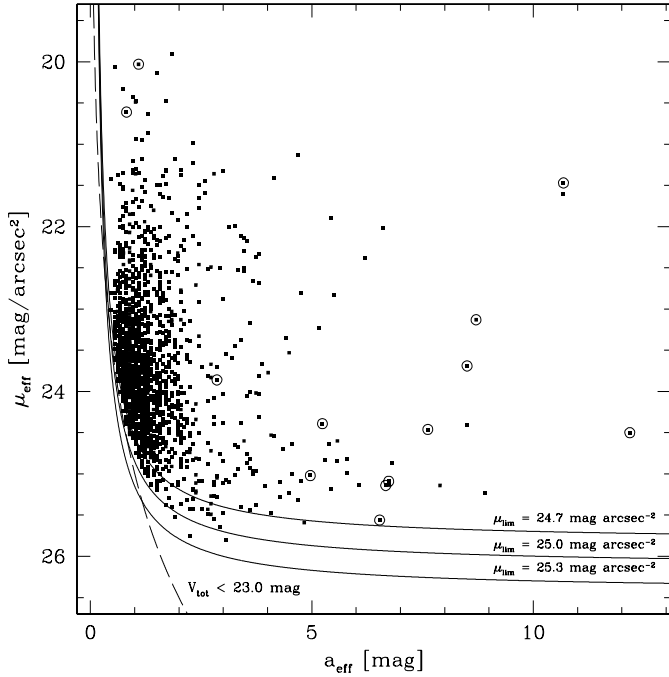


Fig. 6. The effective surface brightness of all galaxies brighter than $V = 23$ mag is plotted versus the effective semi-major axis. Circles indicate Fornax members. The dashed lines show the relation of an exponential law for the limit of the total magnitude. The solid lines are the selection functions for our sample for three typical detection limits (see Table 1) and a limiting radius of $0''.6$. The regions below and left of these limits are inaccessible to our survey

7. Completeness at the Fornax distance

The completeness of a galaxy catalog depends on the following three parameters: limiting magnitude, limiting surface brightness, and limiting scale length. The surface brightness detection limits of the different fields are given in Table 1. They vary between $24.7 < \mu_{\text{lim}} < 25.3$ mag for the central fields. The minimum number of connected pixels for a detection, $n_{\text{min}} = 5$ results in a limiting radius of about $r_{\text{lim}} = 0''.6$. Adopting an exponential law for the galaxy profiles, $\mu(r) = \mu_0 + 1.086(r/\alpha)$, the relation of r_{lim} to μ_{lim} is $r_{\text{lim}} = 0.921 \cdot \alpha(\mu_{\text{lim}} - \mu_0)$. With $r_{\text{eff}} = \alpha/0.5958$ and $\mu_{\text{eff}} = \mu_0 + 1.1245$, the selection function in the μ_{eff} , r_{eff} plane is $\mu_{\text{eff}}(r_{\text{eff}}) = \mu_{\text{lim}} + 1.1245 - 1.8225r_{\text{lim}}/r_{\text{eff}}$. In Fig. 6 all galaxies brighter than $V_{\text{tot}} = 23$ mag are plotted in this plane. The selection functions for three typical detection limits are shown. Objects that are located below and left of these functions are not accessible to our survey.

Figure 7 shows our sample of galaxies in a $\mu_{\text{peak}}-V_{\text{tot}}$ diagram. Note that for most galaxies the μ_{peak} is a lower limit compared to the true central surface brightness as shown in the previous section. Also given are the parameters of Local Group dSphs (Mateo et al. 1993) shifted to the Fornax distance. The limiting μ_{peak} is about 24.0

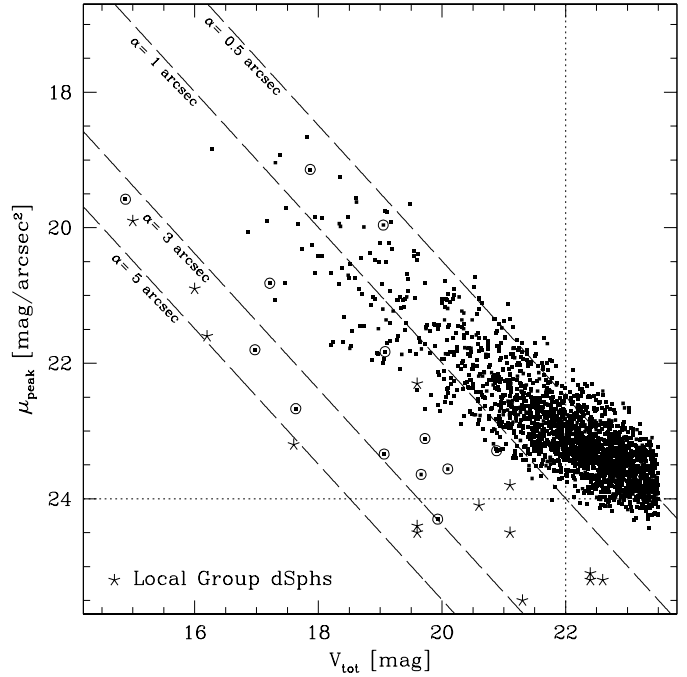


Fig. 7. The peak surface brightness of all galaxies is plotted versus the total V magnitude. The dashed lines show the relation of an exponential law for different scale lengths α . At $V = 22$ mag the completeness starts to drop. The limit in peak surface brightness is about $\mu_{\text{limit}} = 24.0$ mag. Circles indicate Fornax members. The asterisks are the Local Group dwarf spheroidals shifted to the Fornax distance. None of either category falls in the crowded part of the diagram

mag arcsec $^{-2}$. For the V magnitude the galaxy counts start to be incomplete for $V_{\text{tot}} > 22.0$ mag. Concerning dEs in the Fornax cluster which follow the $\mu-V$ relation the completeness starts to drop at even brighter V_{tot} . Thus, for the Fornax dEs we are more restricted in surface brightness than in the absolute magnitude. As shown in Fig. 7, several Local Group dSphs would not have been detected due to their low surface brightnesses, even if their total luminosities would have been within our limits. The dSphs And I and And II, for example, would have total magnitudes of about $V_{\text{tot}} = 19.6$ mag, but central surface brightnesses of $\mu_{0,V} = 24.5$ mag. On the contrary, the dSph Leo I has the same V_{tot} , but a 2 magnitudes brighter $\mu_{0,V}$, which is well within our sample limits.

The resolution limit is given by the seeing conditions. All objects with FWHM larger than $1''.5$, or about 130 pc in Fornax distance, appear resolved. Thus, all Local Group dSphs would appear clearly resolved when shifted to the Fornax distance. The dashed lines in Fig. 7 show the limits for different scale lengths of an exponential law in dependence of V_{tot} and μ_{peak} surface brightness. All objects with scale lengths larger than about $0''.5$ appear resolved.

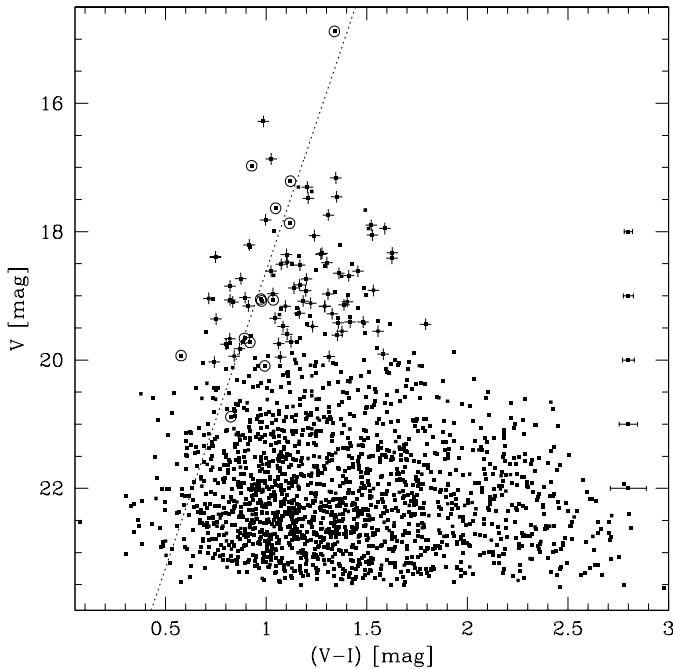


Fig. 8. The plot shows the color magnitude diagram of all galaxies in our CCD fields. The $(V - I)$ colors were measured in apertures with diameters of $3''$. Mean errors are shown on the right. The Fornax dwarf galaxies are encircled. The dashed line is a fit to 8 dEs and dE,Ns from Table 2, excluding the bluest and reddest dwarf. A clear trend is visible in the sense that fainter dEs are bluer, as it is also seen in other clusters (e.g. in Coma, see Secker & Harris 1997). Crosses indicate definite background galaxies according to their radial velocities (see Paper II)

8. Color distribution

In the color magnitude diagram (Fig. 8) all galaxies brighter than $V = 23.5$ mag are shown. Most of the objects have colors of about $(V - I) = 1.2$ mag similar to the average color of the GCSs of the ellipticals in Fornax (Kissler-Patig et al. 1997). Assuming $E(B - V) \simeq 0$ mag towards Fornax, all galaxies redder than $V - I = 1.8$ mag are most likely background galaxies (since no redder stellar populations are expected from any theoretical stellar evolution model, e.g. Worthey 1994). The definite cluster dwarf galaxies (circles) are located at the blue side of the color distribution. Since most of them are early-type dwarfs and show no indications of star formation, their blue colors can only be explained by low metallicities. The dEs and dE,Ns follow a sequence in the sense that fainter galaxies are bluer (see dashed line in Fig. 8). This trend was already noticed by Caldwell & Bothun (1987, who measured UBV magnitudes of 30 relatively bright Fornax cluster dwarf ellipticals) and continues for dwarfs with low surface brightness (Bothun et al. 1991, Cellone et al. 1994). Held & Mould (1994) have shown for 10 nucleated dE,Ns in Fornax that their colors are corre-

Table 3. Average galaxy density per square degree with errors (considering the clustering properties of galaxies) for the different fields in dependence on the limiting V magnitude.

magnitude limit:		$V < 20.0$	$V < 21.0$	$V < 22.0$
Field	R[']	[gal./ \square°]	[gal./ \square°]	[gal./ \square°]
F1 (Ring1)	2.82	2740 \pm 1250	5210 \pm 1720	9880 \pm 2280
F2 (Ring1)	2.82	960 \pm 650	2250 \pm 1010	4180 \pm 1350
F3 (Ring1)	2.82	1250 \pm 850	3330 \pm 1460	
F4 (Ring1)	2.82	1040 \pm 620	2080 \pm 880	4420 \pm 1280
F1 (Ring2)	5.57	1170 \pm 530	2630 \pm 820	6420 \pm 1330
F2 (Ring2)	5.57	1830 \pm 750	3060 \pm 940	7030 \pm 1440
F3 (Ring2)	5.57	1490 \pm 660	2810 \pm 910	
F4 (Ring2)	5.57	420 \pm 270	970 \pm 420	3900 \pm 920
B1	11.54	1050 \pm 420	2200 \pm 620	6320 \pm 1130
N1387	18.24	450 \pm 200	1530 \pm 410	6240 \pm 980
N1427A	21.11	650 \pm 270	2100 \pm 540	4340 \pm 770
N1379	28.08	190 \pm 120	830 \pm 270	2930 \pm 560
N1374	41.96	510 \pm 220	1160 \pm 340	3210 \pm 590
N1427	46.00	790 \pm 310	1660 \pm 460	4040 \pm 730
B2	93.82	550 \pm 220	2180 \pm 530	4430 \pm 740
B3	611.00	310 \pm 80	1400 \pm 210	4290 \pm 420
B4	863.00	640 \pm 150	1940 \pm 310	5120 \pm 540

lated with their metallicities derived from line strengths ($-1.5 < [\text{Fe}/\text{H}] < -0.8$). A color - magnitude relation for dwarf galaxies is also seen in other galaxy clusters, as for example in Virgo (Caldwell 1983, Caldwell & Bothun 1987) or Coma (Secker 1996, Secker & Harris 1997).

No color dependence on the projected distance to the center of NGC 1399 is seen for the dwarfs. Galaxies with actual or recent star formation activity which would stand out by very blue colors cannot be identified. However, some moderately blue galaxies of $V - I \simeq 0.5$ are present. Most of them are located in the background cluster behind the Fornax center (see Paper II) and most likely represent irregular galaxies surrounding ellipticals in this distant cluster. In the center of the Fornax cluster a prominent example of an irregular with this color is NGC 1427A (Hilker et al. 1997).

9. Spatial distribution of the galaxies

We investigated the spatial distribution of all galaxies in order to look for a possible over-abundance of dwarf galaxies in the center of the Fornax cluster. Therefore, we calculated the galaxy densities in the different fields. We define in the following all CCD fields except the NGC 1399 and B1 field as local Fornax background in contrast to the cluster center region. The background fields B3 and B4 were used to estimate the absolute galaxy background counts. The galaxy counts in the central fields F1 - F4 were divided into two rings around the center of NGC 1399, one expanding from $0.4'$ to $4.0'$, the other from $4.0'$ to $7.0'$. Table

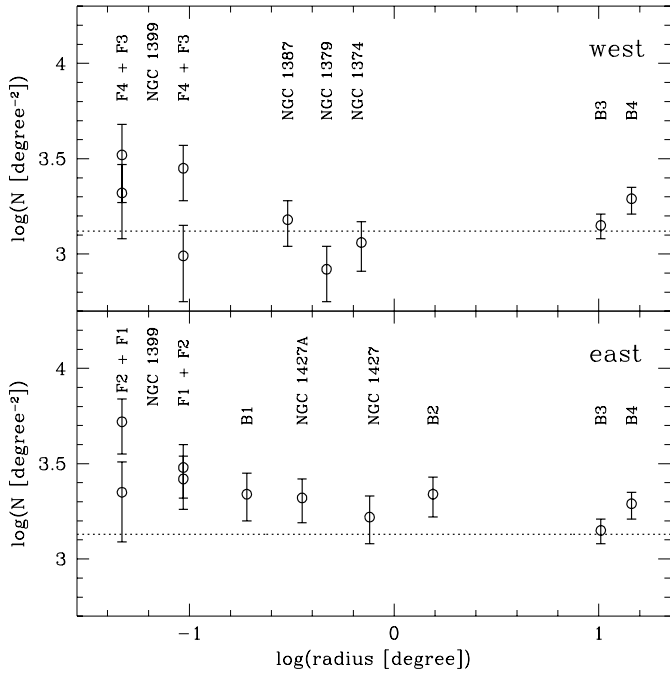


Fig. 9. The galaxy densities for galaxies brighter than $V = 21$ mag are plotted versus the projected radial distance to the central galaxy NGC 1399. The upper panel shows the sequence of fields in west direction, in the lower panel the densities of fields in east direction are plotted. In both panels the densities of the background fields B3 and B4 are given as comparison. An excess population of background galaxies is seen in the central fields. The galaxy density in the eastern fields is on the average higher than in the western fields

3 lists the galaxy density per square degree for the different fields as a function of limiting V magnitude. Note that for magnitudes fainter than $V = 21$ mag the SW field of NGC 1399 (F3) has been omitted due to the shorter exposures in this field. In all the other fields, no incompleteness effects influence the galaxy counts for magnitudes brighter than $V = 22$ mag (see Sect. 7).

The error of the galaxy counts N is a function of the angular correlation $\omega(\theta)$ of galaxies: $\sigma^2 = N + N^2\omega(\theta)$, θ is the size of the field, in which the galaxies have been counted. Values for $\omega(\theta)$ at different limiting V magnitudes were obtained by interpolating the results in Infante & Pritchet (1996), Roche et al. (1993) and Brainerd et al. (1995). We adopted $\omega(1^\circ) = 0.0115 \pm 0.0050$, 0.0056 ± 0.0020 , and 0.0032 ± 0.0010 for $V_{\text{limit}} = 20.0$, 21.0 , and 22.0 mag respectively.

In Fig. 9 we plotted the galaxy densities for galaxies brighter than $V = 21$ mag in relation to the radial distance along the east, respectively west, sequence of our fields with NGC 1399 in the center. The densities of the absolute background fields B3 and B4 are shown as comparison in both directions.

It is striking that the central fields, except F4 and F2 (ring 1), have about 2-3 times higher density values than the other fields. There exists an excess population of galaxies near NGC 1399. Further, the galaxy density in the eastern fields is on the average higher than in the western fields, whose densities are comparable with or even lower than that of the absolute background fields. However, nearly all density values are within the errors that result from the density variations and clustering properties of background galaxies. This makes it nearly impossible to distinguish a possible excess of faint and compact dwarf galaxies, which represent only a few percent of the galaxy counts, from background variations.

The excess of galaxies in the central fields can be explained by a background galaxy cluster at $z = 0.11$ just behind the center of the Fornax cluster. In Paper II we give a detailed analysis of radial velocity measurements of the brightest galaxies in this region. In Fig. 10 we show a galaxy density map of the four central Fornax fields. We constructed this map by counting galaxies with $16.0 < V < 21.5$ mag and $(V - I) < 1.6$ mag in bins of 150×150 pixel (~ 0.32 arcmin²). This sample contains 189 galaxies. The “density pixels” then were smoothed by a 3×3 average filter. Their values range between 0 (white) and 3.5 (black) galaxies per arcmin². Note that the counts in the SW field (F3) and the central “density pixel” are not complete. In the other fields the counts are 100% complete. One can clearly see a banana shaped galaxy distribution east of NGC 1399. Galaxies with observed redshifts of $z = 0.11$ (see also Paper II) match the distribution of high galaxy density very well. We suspect that nearly all excess galaxies in the center belong to the background cluster. Thus, no large excess of dwarf galaxies exists around NGC 1399.

In Fig. 11 we show the distribution of point sources around NGC 1399. We selected all objects with classifier values larger than 0.86, magnitudes between $20.5 < V < 22.0$, and colors in the range $0.6 < (V - I) < 1.6$, in total 248 objects. The isodensity contours have levels between 1.1 and 6.8 objects per arcmin². The contribution of background objects was determined by counting point sources in the local background field B2. With the same selection criteria 0.13 objects per arcmin² have been counted. Thus, about 90% of the point sources should belong to the GCS of NGC 1399 or the background galaxy cluster. Again, the counts in all fields except F3 are 100% complete (see also Kohle et al. 1996). The peak of the distribution is located about 1/3 east of NGC 1399. This result has to be considered with caution, since the counts in the central density pixels as well as in the SW field are not complete. However, we found that this effect also (even more pronounced) occurs when taking brighter samples of point sources, which should not be affected by incompleteness effects. In previous investigations of the GCS of NGC 1399, the properties of GCs in the NE (F2) and NW (F4) field have been examined (Kissler-Patig et al. 1997).

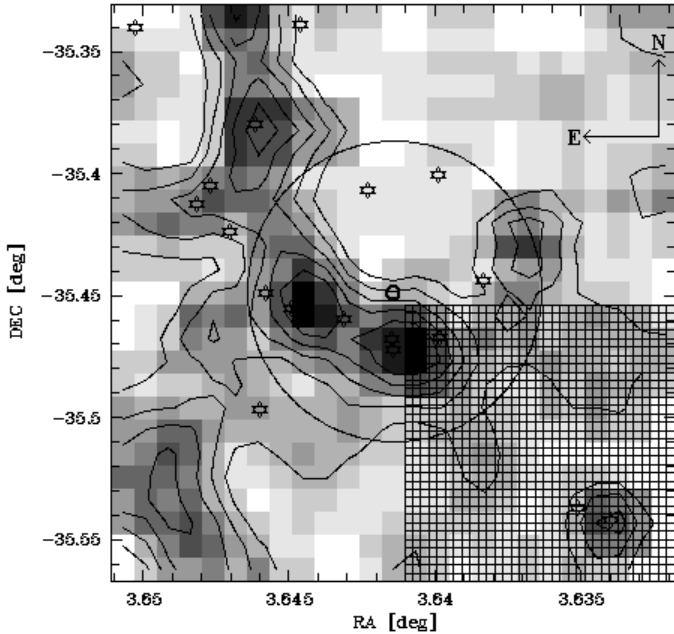


Fig. 10. The grey scale plot is a smoothed density map of galaxies brighter than $V = 21.5$ mag in the central Fornax fields. The circle indicates the location of NGC 1399. Asterisks are galaxies with observed redshift of $z = 0.11$. They match the distribution of high galaxy density very well. The contours correspond to galaxy densities of 2.3, 1.9, 1.6, 1.2, and 0.9 galaxies per arcmin². Note that the counts in the SW field (cross-hatched region) are not complete

We found that the radial surface density profile of the GCs (centered on NGC 1399) is shallower in the NE field than in the NW field. Furthermore Forbes et al. (1998) investigated the angular distribution of GCs within $100''$ (= 5 “density pixels” in a HST WFPC2 image that covers the NE part of the center of NGC 1399). They found a peak in the angular distribution in the east direction. Both results are consistent with our finding of an excess of point sources east of NGC 1399. Note that in this direction also the density of resolved objects is very high.

There are basically three possible explanations for this displacement. First, a significant amount of unresolved galaxies in the background cluster was counted together with the globular clusters. Since the background cluster lies east of NGC 1399 the peak of the distribution of all point sources would then be shifted to the east. In this case, the galaxies would have absolute magnitudes between $-18.0 < M_V < -16.5$ mag and half light radii smaller than about 1.5 kpc assuming a distance of 480 Mpc to the background cluster. Such properties can only be explained by cEs, which are believed to represent only a negligible fraction of the galaxy population in the local universe. In the Fornax cluster, for example, Drinkwater et al. (1997, see also Drinkwater & Gregg 1998) investigated by radial velocity measurements that all galaxies

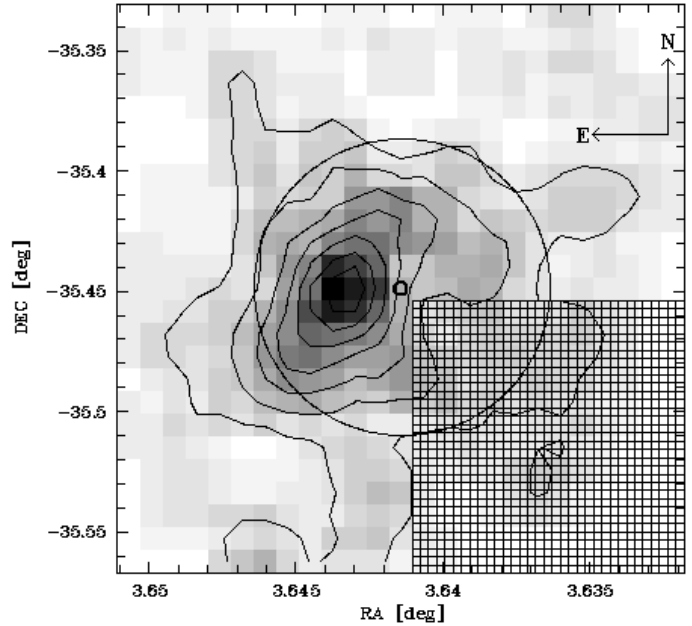


Fig. 11. The same plot as in Fig. 10 for point sources (90% of them are likely globular clusters) between $20.5 < V < 22.0$. The isodensity contours correspond to 6.8, 5.8, 4.9, 3.9, 3.0, 2.1, and 1.1 objects per arcmin². The distribution of point sources seems to be displaced by about $1/3$ to the east of NGC 1399. Note that the counts in the SW field are not complete

in their sample that are classified as M32 type compact ellipticals in the FCC are background galaxies. Further, in the HST counts GCs should be clearly distinguishable from galaxies even at $z = 0.11$. Second, the GCS is really displaced with respect to the bulge of NGC 1399. This would be a hint that the GCS follows another potential than the stellar light and may belong rather to the cluster as a whole than to NGC 1399 itself, as supported by the velocity dispersion measurements in Grillmair et al. (1994) and Kissler-Patig et al. (1998a). In this respect, it is worthwhile noting that the center of the gas distribution detected by X-ray observations is also displaced, to the north-east of NGC 1399 (Ikebe et al. 1996, Jones et al. 1997). Finally, somewhat similar to the latter point, the distribution of GCs might be a temporary displacement of a “normal” GCS centered on NGC 1399. A scenario that supports this possibility is related to the enrichment of the central GCS by the accretion of GCs from other galaxies. Kissler-Patig et al. (1998b) suggest that tidal tails of GCs from the last passage of a Fornax galaxy might still be visible; these could mimic a skewed distribution of GCs around NGC 1399. Further investigations have to show if this riddle can be solved.

10. Summary

In selected fields in the Fornax cluster, located near ellipticals, more than 870 galaxies were identified down to a V magnitude of 22 mag. Photometric properties, such as total V magnitude, $(V - I)$ color, peak and effective surface brightness, and effective radius of these galaxies are compiled in a catalog.

For a bright subsample of the galaxies we determined the seeing corrected true central surface brightnesses. Exponential and/or de Vaucouleur profiles were fitted to these data and their parameters are given in a further catalog (Appendix B). Only few galaxies could clearly be identified as dwarf galaxies by their location in the surface brightness magnitude diagram, where they follow the expected sequence for dwarf ellipticals. Most of them are already listed in the Fornax Cluster Catalog (Ferguson 1989). However, our survey limit of about 24 mag arcsec⁻² in peak surface brightness is too bright to detect dwarfs like the faintest Local Group dwarf spheroidals, if they were located at the Fornax distance. On the other hand, among the high surface brightness objects compact dwarfs might be hidden, as shown by two nucleus-like objects that are Fornax members as derived from their radial velocities (see also Paper II).

The “ n ” parameter of the Sérsic profile fits is clearly correlated to the absolute luminosity of the dwarf ellipticals in Fornax. The n -luminosity relation seems to continue in the region of the “normal” ellipticals.

In the color magnitude diagram the dwarfs tend to follow a color – magnitude relation in the sense that fainter galaxies are bluer. The common explanation for this relation is a decreasing metallicity with decreasing luminosity. However, for some dwarfs the blue colors might also be a hint for an existing young or intermediate-age stellar population, as it is seen in several Local Group dwarf spheroidals. Evident signs for recent and ongoing star formation in the center of the cluster can only be seen in the irregular galaxy NGC 1427A.

At fixed limiting magnitude the galaxy density strongly varies from field to field. On average the density in most fields is comparable to the one in the absolute background fields. South and east of NGC 1399 we found a significant excess of galaxies as compared to the other fields. However, an excess of dwarf galaxies surrounding NGC 1399 can be ruled out, since nearly all of these galaxies belong to a background cluster at $z = 0.11$. The brightest galaxy of this background cluster possesses an extended cD halo and is located 1'1 south of NGC 1399. The strong background galaxy fluctuations make the search for compact dwarfs by a statistical subtraction of background objects meaningless.

The point sources in the central Fornax fields are not uniformly distributed around NGC 1399. The peak of their density distribution is displaced about 1/3 east of the center of the galaxy. Assuming that most of them are no back-

ground cluster members, but rather globular clusters, two explanations seem to be possible: (1) the central globular cluster system and the bulge of NGC 1399 are disentangled from each other and follow different potentials, or (2) tidal tales of accreted globular clusters from passing Fornax galaxies have temporarily squewed the distribution of globular clusters.

Acknowledgements. We thank the referee H.C. Ferguson for his very useful comments which improved the paper. This research was partly supported by the DFG through the Graduiertenkolleg ‘The Magellanic System and other dwarf galaxies’ and through grant Ri 418/5-1 and Ri 418/5-2. LI and HQ thanks Fondecyt Chile for support through ‘Proyecto FONDECYT 8970009’ and from a 1995 Presidential Chair in Science.

Appendix

The two catalogs given in this Appendix are available in electronic form only at the CDS via anonymous ftp to cdsar.u-strasbg.fr (130.79.128.5) or via <http://cdsweb.u-strasbg.fr/Abstract.html>. The photometric catalog contains observational data for all galaxies ($V < 22.0$) in the central Fornax fields. The second catalog contains the parameters of fits to the surface brightness profiles of a subsample of the photometric catalog. In both catalogs the objects are sorted in order of increasing right ascension. In the following we describe the columns of the catalogs.

Appendix A: The photometric catalog

Column 1. Identification of the object. It is prefixed by the acronym CGF (Catalog of Galaxies in Fornax) followed by a sequence number of the field and the sequence number of the galaxy in this field (ordered with decreasing magnitude). For example, CGF 5-12 is the 12th brightest galaxy in field 5 (see also Sect. 2.1).

Column 2. Right ascension for the epoch 2000 in hours, minutes and seconds (^{h} , ^{m} , ^{s}).

Column 3. Declination (2000) in degrees, minutes and seconds (^{$^{\circ}$} , ^{$'$} , ^{$''$}).

The positions of all objects were determined relative to positions in the Guide Star Catalog. Typically 4 to 8 catalog positions are found in each field. Coordinate transformations with 3 plate constants have been obtained. The positional accuracy of the calculated coordinates is in all fields better than 0.3".

Column 4. Total V apparent magnitude as determined by SExtractor, see Sect.4. Values with an appended 'n' indicate that neighboring objects are present within 2 isophotal radii.

Column 5. V peak surface brightness in mag arcsec⁻² as given by SExtractor (not seeing corrected).

Column 6. $(V - I)$ colors within an aperture of 3" in diameter.

Column 7. Ellipticity of the galaxy and the used elliptical aperture, defined as $\epsilon = 1 - b/a$.

Table A.1. Cross references to other catalogs

	NGC	C87	F89	D88&I90
CGF 9-1			B1016	231
CGF 9-5			FCC141	
CGF 9-6		NG123	FCC145	230
CGF 9-12			FCC154	
CGF 8-1		NG16	FCC160	238
CGF 8-3			FCC162	
CGF 4-1	1396		FCC202	
CGF 3-1			B1241	95
CGF 3-2		NG21	FCC208	257
CGF 3-3			B1237	
CGF 3-6				258
CGF 3-7			B1220	
CGF 1-10				266
CGF 10-2			B1571	
CGF 10-13			FCC272	

Column 8. Position angle of the major axis of the elliptical aperture. 0 degree is in east direction, positive angles towards the south, and negative angles towards the north direction.

Column 9. Size of the major axis of the elliptical aperture in arcsec. Note that the limiting isophote of the ellipse slightly varies from field to field depending on the seeing and sky brightness.

Column 10. Size of the major axis at an isophotal surface brightness of $\mu_V = 26$ mag in arcsec, D_{26} .

Column 11. Effective semi-major axis a_{eff} in arcsec. Major axis containing half of the total light measured in elliptical apertures.

Column 12. Effective surface brightness μ_{eff} , mean surface brightness within the effective semi-major axis.

A.1. Crossreferences to other catalogs

Some of our galaxies are also listed in previous catalogs. Table 4 gives cross references for these galaxies. The abbreviations are as follows: C87 = Caldwell (1987), F89 = Ferguson (1989, Fornax Cluster Catalog), D88&I90 = Davies et al. (1988) and Irwin et al. (1990).

Appendix B: Catalog of profile fit parameters

Column 1. Identification name as in Appendix A.

Column 2.+3. Right ascension and declination (epoch 2000.0) as in Appendix A.

Column 4. Galaxy type as determined by morphological classification and analysis of surface brightness profiles.

Column 5. Total V magnitude as in Appendix A.

Column 6. Apparent core radius $r_{c,\text{app}}$ in arcsec (= radius where the apparent central surface intensity has its half value).

Column 7. Corrected core radius $r_{c,\text{cor}}$ in arcsec (using Kormendy’s correction 1985).

Column 8. Corrected central surface brightness $\mu_{0,\text{cor}}$ in V (using Kormendy’s correction 1985).

Column 9. Exponent n of Sersic profile fit.

Column 10. Central surface brightness $\mu_{0,\text{Sersic}}$ in V of Sersic profile fit.

Column 11. Scale length $r_{0,\text{Sersic}}$ of Sersic profile fit in arcsec.

Column 12. Central surface brightness $\mu_{0,\text{dV}}$ of a de Vaucouleurs profile fit.

Column 13. Effective radius $r_{\text{eff,dV}}$ of the de Vaucouleurs fit in arcsec. Radius, where the surface brightness is two times fainter than in the center.

Column 14. Central surface brightness $\mu_{0,\text{exp}}$ of an exponential law.

Column 15. Scale length α of an exponential law in arcsec.

Column 16. Flag for the exponential profile fit indicating, if a bulge “b” is present, a light deficiency in the center “d”, a nucleus “n”, or if the profile follows an exponential law at all radii “e”.

References

- Bertin E., 1995, SExtractor 1.0 User’s Guide
 Bertin E., Arnouts S., 1996, A&AS 117, 393
 Binggeli B., 1994, in: ESO/OHP Workshop on Dwarf Galaxies, eds. G. Meylan & P. Prugniel, ESO, Garching
 Bothun G.D., Impey C.D., Malin D.F., 1991, ApJ 376, 404
 Brainerd T.G., Smail I., Mould J., 1995, MNRAS 275, 781
 Bridges T.J., Hanes D.A., Harris W.E., 1991, AJ 101, 469
 Caldwell N., 1983, AJ 88, 804
 Caldwell N. L., Bothun G.D., 1987, AJ 94, 1126
 Caldwell N., Armandroff T., Seitzer P., Da Costa G., 1992, AJ 103, 840
 Cellone S.A., Forte J.C., 1996, ApJ 461, 176
 Cellone S.A., Forte J.C., Geisler D., 1994, ApJS 93, 397
 Davies J.I., Phillipps S., Cawson M.G.M., Disney M.J., Kibblewhite E.J., 1988, MNRAS 232, 239
 Della Valle M., Kissler-Patig M., Danziger J., Storm J., 1998, MNRAS in press
 de Vaucouleurs G., 1948, Ann. d’Astrophys. 11, 247
 Drinkwater M.J., Gregg M.D., 1998, MNRAS 296, L15
 Drinkwater M.J., Gregg M.D., Holman B.A., 1997, in ASP Conf. Series, Vol. 116, Proceedings of the Second Stromlo Symposium ‘The Nature of Elliptical Galaxies’ Eds. M. Arnaboldi, G.S. Da Costa & P. Saha
 Ferguson H.C., 1989, AJ 98, 367
 Forbes D.A., Grillmair C.J., Williger G.M., Elson R.A.W., Brodie J.P., 1998, MNRAS 293, 325
 Graham A., Lauer T.R., Colless M., Postman M., 1996, ApJ 465, 534
 Gratton R.G., Fusi Pecci F., Carretta E., Clementini, Corsi C.E., Lattanzi M.G., 1997, in: “Hipparcos Venice’97 Symposium”, ESA SP-402
 Grillmair C.J., Freeman K.C., Bicknell G.V., Carter D., Couch, W.J., Sommer-Larsen J., Taylor K., 1994, ApJ 422, L9
 Hanes D.A., Harris W.E., 1986, ApJ 309, 564

- Held E.V., Mould J.R., 1994, *AJ* 107, 1307
- Hilker M., Bomans D.J., Kissler-Patig M., Infante L., 1997, *A&A* 327, 562
- Hilker M., Infante L., Vieira G., Kissler-Patig M., Richtler, T., 1998, *A&AS*, (Paper II)
- Hilker M., Richtler, T., Infante L., Kissler-Patig M., 1998, *A&A*, in preparation (Paper III)
- Ikebe Y., Ezawa H., Fukazawa Y. et al., 1996, *Nature* 379, 427
- Infante L., 1987, *A&A* 183, 177
- Infante L., Pritchett C.J., 1996, *ApJ*, 439, 565
- Irwin M.J., Davies J.I., Disney M.J., Phillipps S., 1990, *MNRAS* 245, 289
- Jerjen H., Binggeli B., 1997, in *ASP Conf. Series*, Vol. 116, Proceedings of the Second Stromlo Symposium ‘The Nature of Elliptical Galaxies’ Eds. M. Arnaboldi, G.S. Da Costa & P. Saha
- Jones C., Stern C., Forman W., Breen J., David L., Tucker W., Franx M., 1997, *ApJ* 482, 143
- Killeen N.E.B., Bicknell G.V., 1988, *ApJ* 325, 165
- Kissler-Patig M., Kohle S., Hilker M., Richtler T., Infante L., Quintana H., 1997, *A&A* 319, 470
- Kissler-Patig M., Brodie P.B., Schroder L.L., Forbes D.A., Grillmair C.J., Huchra J.A., 1998a, *AJ* 115, 105
- Kissler-Patig M., et al., 1998b, *AJ*, in preparation
- Kohle S., Kissler-Patig M., Hilker M., Richtler T., Infante L., Quintana H., 1996, *A&A* 309, L39
- Kormendy J., 1985, *ApJ* 295, 73
- Kron R.G., 1980, *ApJS* 43, 305
- Landolt A.U., 1992, *AJ* 104, 340
- López-Cruz O., Yee H.K.C., Brown J.P., Jones C., Forman W., 1997, *ApJ* 475, L97
- Mateo M., Olszewski E.W., Pryor C., Welch D.L., Fischer P., 1993, *AJ* 105, 510
- Prugniel P., Bica E., Klotz A., Alloin D., 1993, *A&AS* 98, 229
- Roche N., Shanks N., Metcalfe N., Fong R., 1993, *MNRAS* 262, 360
- Sandage A., Binggeli B., 1984, *AJ* 89, 919
- Schombert J.M., 1986, *ApJS* 60, 603
- Schweizer F., 1981, *AJ* 86, 662
- Secker J., 1996, *ApJ* 469, L81
- Secker J., Harris W.E., 1997, *ApJ* 469, 623
- Sérsic J.-L., 1968, *Atlas de galaxias australes*, Observatorio Astronómica, Córdoba
- Wagner S.J., Richtler T., Hopp U., 1991, *A&A* 241, 399
- Worthey G., 1994, *ApJS* 95, 107
- Young C.K., Currie M.J., 1994, *MNRAS* 268, L11

This figure "fig1.gif" is available in "gif" format from:

<http://arxiv.org/ps/astro-ph/9807143v1>